Journal of Biomolecular NMR (2006) 36: 45–54
DOI 10.1007/s10858-006-9066-1


*Article*

# Processing of ND NMR spectra sampled in polar coordinates: a simple Fourier transform instead of a reconstruction

Dominique Marion*
*Institut de Biologie Structurale "Jean-Pierre Ebel", CNRS-CEA-UJF, 41, Rue Jules Horowitz, 38027, Grenoble Cedex 1, France*

Received 31 March 2006; Accepted 11 July 2006

*Key words:* digital resolution, Fourier transformation, non-linear sampling, polar coordinates

**Abstract**

In order to reduce the acquisition time of multidimensional NMR spectra of biological macromolecules, projected spectra (or in other words, spectra sampled in polar coordinates) can be used. Their standard processing involves a regular FFT of the projections followed by a reconstruction, i.e. a non-linear process. In this communication, we show that a 2D discrete Fourier transform can be implemented in polar coordinates to obtain directly a frequency domain spectrum. Aliasing due to local violations of the Nyquist sampling theorem gives rise to base line ridges but the peak line-shapes are not distorted as in most reconstruction methods. The sampling scheme is not linear and the data points in the time domain should thus be weighted accordingly in the polar FT; however, artifacts can be reduced by additional data weighting of the undersampled regions. This processing does not require any parameter tuning and is straightforward to use. The algorithm written for polar sampling can be adapted to any sampling scheme and will permit to investigate better compromises in terms of experimental time and lack of artifacts.

*Abbreviations:* FFT – fast Fourier transform; LP – linear prediction; MEM – maximum entropy method; S/N – signal-to-noise ratio

## Introduction

Recent advances in magnetic field and probe sensitivity have contributed to increase the size of proteins (Tugarinov et al., 2002) amenable to an NMR study but surprisingly much less to reduce the experimental time devoted to sample the set of multidimensional NMR spectra needed for resonance assignment and structure determination. As a matter of fact, 3D and 4D NMR spectra are generally collected in a traditional manner by monitoring all the chemical shift evolutions independently and processing the spectra with fast Fourier transform (FFT).

*To whom correspondence should be addressed. E-mail: Dominique.Marion@ibs.fr

A multidimensional experiment can be shortened by incrementing several delays in a correlated manner, as suggested initially in the "accordion" experiment (Bodenhausen and Ernst, 1982). A frequency was monitored during one of these delays and a exchange process (along the longitudinal axis) during the other. A minor conceptual modification (i.e. sampling two frequencies) has led to the reduced dimensionality spectroscopy (Szyperski et al., 1993; Simorre et al., 1994; Szyperski et al., 2002; Bersch et al., 2003). It can be combined with other time-saving approaches such as non linear sampling, selective/Hadamard excitation (Kupče et al., 2003; Van Melckebeke et al., 2004) and with alternate processing techniques LP (Gesmar et al., 1990), MEM (Rovnyak et al.,

2004), FDM (Chen et al., 2004), Multiway Decomposition (Malmodin and Billeter, 2005). Distinction should be made between direct (or deterministic) and search (or iterative) processing algorithms (see Yoon et al., 2006 for discussion). The Fourier transform belongs to the first class, which requires little expertize to use and always leads to a reasonable result. In contrast, any iterative scheme is more challenging to use as it may diverge and fail. Although some search algorithms may lead to *better* spectra, we will deliberately limit our discussion of direct methods.

In this paper, we describe a simple linear processing method based on Fourier transform that leads to spectra that can be interpreted quantitatively. It is based on the strategy introduced in the mid-1990s which aims at reducing the number of sampled points in a ND experiment while trying to preserve the spectral resolution: it is known under a number of different names such as reduced dimensionality, G-matrix FT NMR or projection spectroscopy. By conflating two evolution periods, a correlation spectrum between $N$ nuclei can be sampled in a (N − 1)D spectrum: weighted sums and differences of NMR frequencies are obtained. This atypical feature is sometimes considered as inconvenient for a graphical interpretation of the data. To alleviate this drawback, reconstruction methods were introduced to build a ND spectrum from *several* projected (N − 1)D, (N − 2)D, ... spectra. If a large number of projections is acquired, the experiment dimensionality and overall time is no longer changed, but only its sampling scheme (polar instead of Cartesian): in other words, it can thus be referred to as a *polar sampling method*.

Widely used in disparate research fields such as astronomy and medical imaging, projection-reconstruction (PR) aims at finding the ND spectrum compatible with the measured projections, by means of inverse Radon transform, empirical backprojection schemes or iterative procedures. If the experimental sensitivity is good enough, the lower-value (LV) reconstruction (Kupče and Freeman, 2004a) can be used. While the base plane noise is reduced, the reconstructed spectrum exhibits the signal-to-noise of a single projection and a peak missing in one projection will not be reconstructed. In contrast, the backprojection method (BP) proposed by Kupče and Freeman (2004b) is an additive reconstruction algorithm that enjoys the benefit of the signal accumulation of the full experiment. It can produce significant artifacts when used with a limited set of projections. To counterbalance these drawbacks, a hybrid method (combining BP and LV) was recently proposed by Venters et al. (2005).

We have shown in a previous paper (Marion, 2005) that 1D data sampled on a non-uniform grid could be Fourier transformed after a Lagrange interpolation. The polar sampling method leads to data sampled in a non-linear two-dimensional manner. Unfortunately, interpolation using Lagrange polynomial cannot be extended to two dimensions. Alternatively, we propose here to use a direct numerical *integration* of the Fourier transform. Non-linear sampling methods aim at maximizing the spectral resolution for a given amount of experimental time or conversely to minimize the latter for a given resolution. One should keep in mind that there is no way to achieve this goal without violating the Nyquist sampling theorem at one place or another. Consequently, the resulting spectrum will exhibit a lower signal-to-noise ratio than a standard one and may contain artifacts. A balance has to be found between positive and negative aspects.

While this work was is progress, Kazimierczuk et al. (2006) have independently proposed a related FT-based method to process arbitrarily sampled data points. Although the two techniques share some basic principles, we will show that their practical implementation differs as well as their range of applicability.

## Materials and methods

In a regular 3D experiment, the signal is sampled along a Cartesian grid $\{t_1, t_2, t_3\}$, where $t_1 = n_1 \times \Delta t_1$, $t_2 = n_2 \times \Delta t_2$, $t_3 = n_3 \times \Delta t_3$ and $n_1, n_2, n_3 \in \mathbb{N}$. Note that complex pairs have to be sampled along each dimension for quadrature purpose. In the polar sampling method, the signal is measured at the following points: $\{t_1 \times \cos(\alpha_2), t_1 \times \sin(\alpha_2), t_3\}$, where $(\alpha_2 = \lambda_2 \times \Delta\alpha_2)$, $n_1$, $\lambda_2$, $n_3 \in \mathbb{N}$ and $0 \leq \alpha_2 \leq \pi/2$. As the difference between the two schemes boils down to a coordinate change, the discrete Fourier transform has to be rewritten in a different coordinate system.

Let us start from the continuous 2D Fourier transform

$$F(\nu_1,\nu_2)=\int_{-\infty}^{\infty}\int_{-\infty}^{\infty} f(t_1,t_2)\exp(-2\pi i\nu_1 t_1)\times\exp(-2\pi\tilde{i}\nu_2 t_2)dt_1dt_2 \quad (1)$$

where symbol $\tilde{i}$ is used to denote the square root of $(-1)$ for the second dimension. This formal notation is essential for the practical implementation of the 2D FT in order to distinguish the complex pairs along the two dimensions.

In the case of a discrete 2D transform, the double integral of Equation 1 is replaced by a double *weighted* sum and two coordinate systems for the sampled data are considered (cf. Figure 1): a Cartesian grid and a polar grid.

Starting from a $(M\times N)$ time-domain matrix sampled on a Cartesian grid, the *discrete* 2D transform is calculated as:

$$F(\nu_1^m,\nu_2^n)=\sum_{j=0}^{M-1}\sum_{k=0}^{N-1} f(t_1^j,t_2^k)B_{jk}^{mn}\cdot\Delta t_1^{\,j}\cdot\Delta t_2^k \quad (2)$$

where

$$B_{jk}^{mn}=\exp(-2\pi i\nu_1^m t_1^j)\cdot\exp(-2\pi\tilde{i}\nu_2^n t_2^k) \quad (3)$$

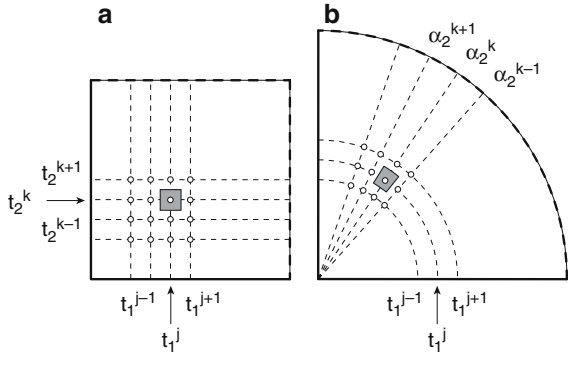


*Figure 1.* Cartesian and polar sampling schemes. In Cartesian sampling, both time variables ($t_1^j$ and $t_1^k$) are independently incremented in a linear manner ($\Delta t_1^{\,j}$ and $\Delta t_1^k$). The initial value might be set to 0 or shifted by half the dwell-time ($1/(2\times SW_1)$ or $1/(2\times SW_2)$ respectively). In polar sampling a radial (time) coordinate ($t_1^j$) and a polar coordinate ($\alpha_2^k$) are used and converted into time variables $t_1^j\times\cos(\alpha_2^k)$ and $t_1^j\times\sin(\alpha_2^k)$ (the same spectral width is here used for both dimensions). $0°<\alpha_2^k<90°$. The same time increment is used for both schemes and $SW_1 = SW_2$. The shaded area corresponds to the integration area for each data point. Whereas this area does not change in Cartesian sampling, it has to be evaluated for each point for polar sampling: defining $\Delta t_1^{\,j}=t_1^{j+1}-t_1^j$ and $\Delta\alpha_2^k=\alpha_2^{k+1}-\alpha_2^k$, the integration area can be approximated as $S^{jk}\approx\Delta t_1^{\,j}(t_1^j\times\Delta\alpha_2^k)$.

Becausethe data are equispaced in the time domain (cf. Figure 1),

$$F(\nu_1^m,\nu_2^n)=\sum_{j=0}^{M-1}\sum_{k=0}^{N-1} f(t_1^j,t_2^k)B_{jk}^{mn} \quad (4)$$

Note that one can compute a $(M'\times N')$ frequency domain matrix $(0\le m<M'$ and $0\le n<N')$. However, if $M'\neq M$ and $N'\neq N$, some spectral leakage or cross-talk can occur because the discrete FT assumes that the input signal is the same as its periodic extension.

Let us express the 2D transform as a processing scheme starting from time-domain data in *polar* coordinates (as defined in Figure 1) and leading to a frequency domain data in *Cartesian* coordinates. The running variables in the time domain should be replaced by:

$$t_1^j\rightarrow t_1^j\cos(\alpha_2^k)\quad t_2^k\rightarrow t_1^j\sin(\alpha_2^k) \quad (5)$$

and the integration area for this point (gray shaded area in Figure 1)

$$S^{jk}=\Delta t_1^{\,j}\cdot(t_1^j\Delta\alpha_2^k) \quad (6)$$

Thus, the 2D FT can be expressed as:

$$F(\nu_1^m,\nu_2^n)=\sum_{j=0}^{M-1}\sum_{k=0}^{N-1} f(t_1^j,\alpha_2^k)A_{jk}^{mn}\cdot\Delta t_1^{\,j}\cdot(t_1^j\Delta\alpha_2^k) \quad (7)$$

with

$$A_{jk}^{mn}=\exp(-2\pi i\cdot\nu_1^n t_1^j\cos(\alpha_2^k))\cdot\exp(-2\pi\tilde{i}\cdot\nu_2^m t_1^j\sin(\alpha_2^k)) \quad (8)$$

If we assume that the angular coordinates ($\alpha_2^k$) are equispaced, the integration area $S^{jk}$ can be computed from the area difference of two concentric disks:

$$S^{jk}=\frac{\pi}{16N}\left[\left(t_1^{j+1}+t_1^j\right)^2-\left(t_1^j+t_1^{j-1}\right)^2\right] \quad (9)$$

If the radial coordinates ($t_1^j$) are also equispaced, Equation 9 can be simplified as:

$$S^{jk}=S^j=\frac{\pi}{4N}(2j+1)\cdot\Delta t_1 \quad (10)$$

Let us note that $F(\nu_1^m,\nu_2^n)$ defines an hypercomplex term and that only the real–real component will be kept once the spectrum has been properly phased.

These expressions were implemented in a computer program written in C-language interfaced with the *nmrPipe* processing suite (Delaglio et al., 1995). As a test case, a HNCO experiment was recorded on a 0.5 mM sample of human ubiquitin (pH = 6.2) on a Varian Inova 600 spectrometer using the BioPack "ghn_coA" pulse sequence. To evaluate the robustness of all processing schemes, the experimental data sets were processed twice, once with addition of Gaussian noise and once unaltered. The amount of noise added leads to a 10-fold decrease of S/N in the Cartesian spectrum processed with FFT.

The time-domain HNCO data were first transformed along $t_3$ using FFT (using nmrPipe). Along $t_1$ and $t_2$, the Cartesian data set is then processed in a conventional manner (FFT using nmrPipe) and the polar data sets using several reconstruction methods (BP, LV, HBLV with bin size of 4) and using our algorithm. For Cartesian sampling $48 \times 48$ increments ($t_1^j$, $t_2^k$) were used and for polar sampling, 128 radial ($t_1^j$) increments and 18 angular increments ($\alpha_2^k = 2.5°, 7.5°, \ldots$). The $^{15}$N and $^{13}$C spectral widths are set to 2200 Hz except for the reconstructed spectra where a constant width of 3100 Hz was chosen to permit reconstruction over 2200 Hz (3100 Hz = $\sqrt{2} \times$ 2200 Hz). The 3D acquisition time is 13 h and the processing times for one $^{15}$N–$^{13}$C-plane (iMac G5 2.0 GHz) are 280 s (polar FT), $<5$ s (FFT), $<10$ s (LV) and 750 s (HBLV).

## Results and discussion

We have derived the analytical expression for the 2D FT in polar coordinates to permit comparison with other techniques used such as reconstruction. Note that any non-linear 2D sampling scheme could be handled with our method, provided that the above expressions are recasted accordingly. To reconstruct 2D spectra starting from 1D projections, two alternative approaches have been proposed where a provisional 2D spectrum is combined successively by all 1D projections. For spectra with good sensitivity, this process selects the LV method while for spectra with poor sensitivity an addition is performed (BP method). The former method (LV) is a non-linear processing operation, which tends to reduce the baseplane noise level, but does not lead to any signal accumulation. Thus, the reconstructed spectrum has the same S/N ratio as any individual projection. In contrast, the additive BP method benefits from the signal-to-noise ratio of the complete experiment but with the drawback of significant broadening as well as ridges and ghost peaks well above the noise level across the entire reconstructed spectrum. Both kinds of artifacts can be reduced by applying a stronger window function, as shown by Coggins et al. (2005). As we aim at improving the spectral resolution, we will not discuss the BP method any further in this paper. To reconstruct weak cross-peaks with signal accumulation and without the introduction of artifacts, Venters et al. (2005) have proposed the Hybrid Back-Projection/Lower Value HBLV algorithm which uses a two-step reconstruction process, namely, a BP step followed by an LV step. First, the projections are grouped into bins for which a BP reconstruction is computed. All BP reconstructions are then compared by LV, and the lowest of the reconstructed intensities is retained. Unfortunately, this algorithm is highly computational demanding as compared to the simple BP and LV one.

Figure 2 shows a $^{15}$N–$^{13}$C plane of the HNCO experiment recorded using Cartesian (inset b) and polar sampling (all other panels). Keeping in mind that processing algorithms that perform well on high-quality spectra may eventually fail when the signal-to-noise ratio drops significantly, we here show experimental data on a 0.5 mM sample of Ubiquitin to which Gaussian noise was artificially added. The original spectrum will be used later on as a reference to evaluate the linearity of the processing. This aims at simulating less favorable experimental conditions, such as larger proteins with broader signals or less sensitive triple resonance experiments (i.e. including more coherence transfers than HNCO). The plane shown in Figure 2 was selected because of the two overlapping signals which can only be resolved if the spectral resolution is high enough.

The result of a direct 2D FT using data sampled in polar coordinates in Figure 2a can be first compared with the Cartesian sampling shown in Figure 2b. A higher resolution but a lower S/N is observed for the spectrum in Figure 2a. These differences in resolution and noise level are primarily due to the acquisition scheme rather than to the processing algorithm. A longer acquisition time (128 radial increments vs. 48 increments, with the same dwell time) leads to better spectral

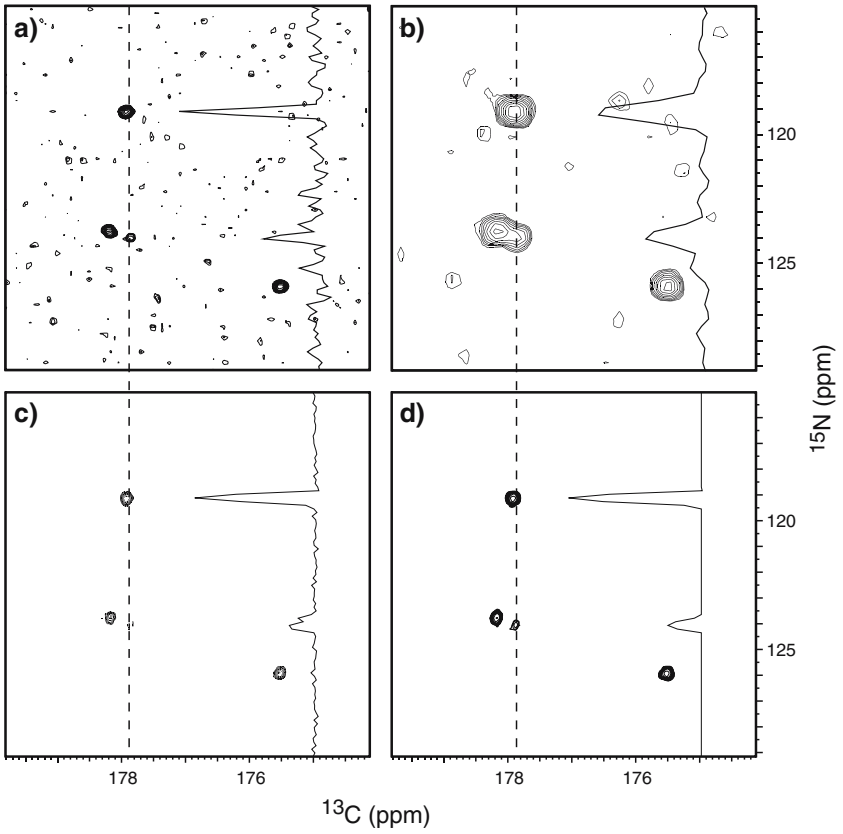


*Figure 2.* Comparison of $^{15}$N–$^{13}$C planes taken at $^{1}$H = 8.54 ppm in a HNCO recorded on human ubiquitin using polar sampling (inset a, c and d) and Cartesian sampling methods (inset b). Gaussian noise was added to the time-domain data (see text). After a standard FFT along the detection dimension, spectrum b) has been processed using apodization and FFT (nmrPipe), spectra (a) using the algorithm described in the text, spectra (c), (d) using reconstruction methods (c = lower-value LV, d = HBLV with bin size of 4). The displays do not correspond to the full spectral widths. The lowest level for each contour plot corresponds to 10% of the amplitude of the upper left cross-peak and the 1D cross-section is taken at the position of the dotted line.

resolution, but a lower S/N because of relaxation effects. Using Cartesian sampling ($128t_1 \times 128t_2$) the same resolution can be reached with a 7-fold increase in spectrometer time. Note that the $^{13}$C dimension is not sampled in a constant time-manner whereas the $^{15}$N dimension uses a semi-constant time method (Van Doren and Zuiderweg, 1994).

Using the polar sampling data set, spectra were reconstructed using the BP (data not shown), LV (Figure 2c) and HBLV (Figure 2d) methods. The BP method gives rise to much broader signals than the LV approach, all other parameters being identical. In the case of LV, all signals display a polygonal character (already noticed by Kupče and Freeman, 2004a) and weaker peaks exhibit distorted line shape, splitting (cf. the 1D cross-section of Figure 2) or altered amplitude. This non-linear behavior may lead to misassignment or erroneous peak quantification. Note that the distortion of the weaker signals is partially reduced using the hybrid method (Venters et al., 2005), at the expense of the processing time requirements. As far as the noise is concerned, it is also reduced in a non-linear manner in the LV method and cannot be used reliably to define a confidence interval during peak picking. In contrast, our FT algorithm in polar coordinates is a linear method that leads to a realistic noise pattern.

Let us now analyze how the polar FT and the reconstruction methods behave when the experimental noise changes or when the number of data points in the angular direction is modified. In Figure 3 are displayed the outcome of the three methods (polar FT, HBLV and LV) for the same plane as in Figure 2: in the left column are

displayed the HNCO spectra with added noise (as in Figure 2), in the center one the original HNCO spectra (with 128 radial ($t_1^j$) increments and 18 angular increments ($\alpha_2^k$)) and in the right column a reduced HNCO data set with only six angular increments. Because the relative scale of these spectra varies as well as the noise base plane, we have chosen to plot the first contour level at 10% of the amplitude of the upper left cross-peak. In the reconstructed spectra (Figure 3d vs. 3e, and Figure 3g vs. 3h), the relative intensity of the cross-peaks changes with the experimental noise,

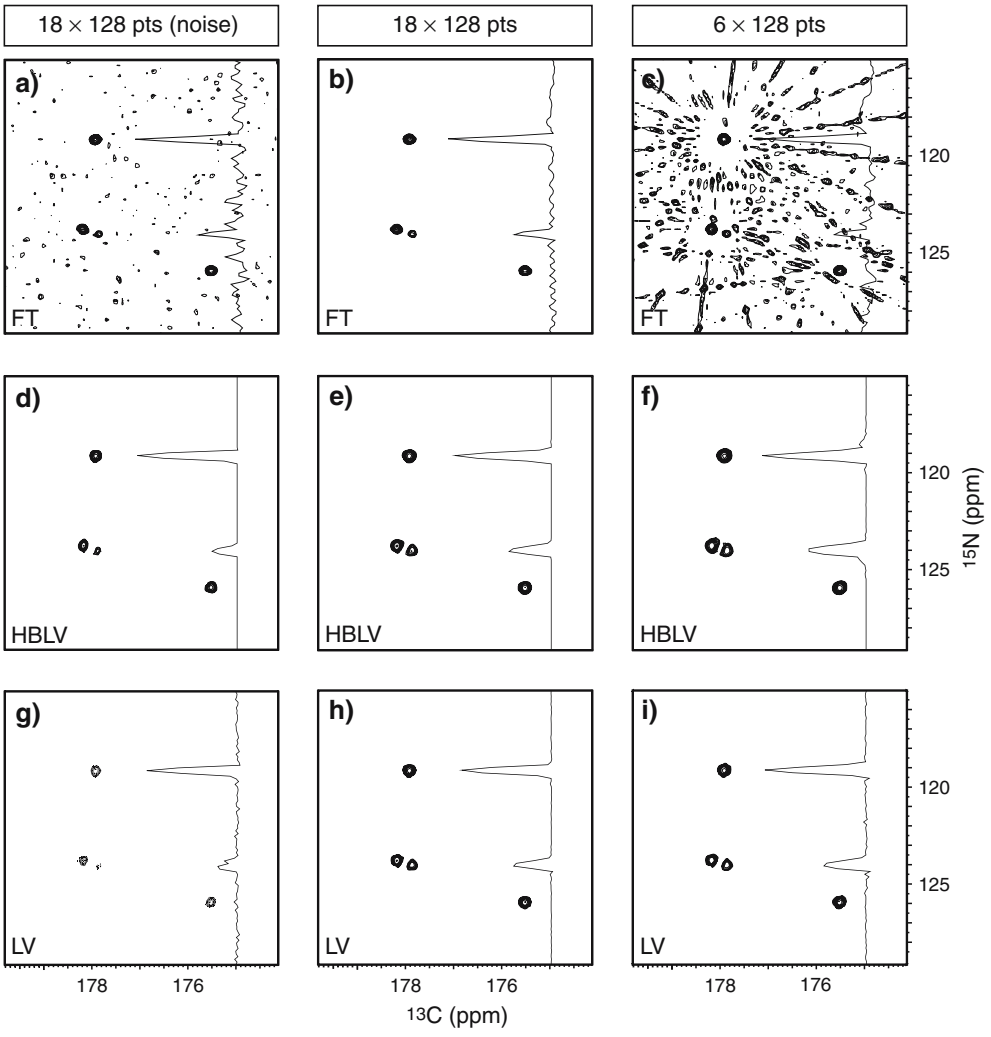


*Figure 3*. Influence of the experimental noise and of the number of projections (angular increments) when processing data sampled in polar coordinates. Two HNCO spectra were recorded using polar sampling (spectral width of 2200 for polar FT and 3100 Hz for reconstruction). The original data are shown in the central column, spectra (b), (e) and (h). Using the "*addNoise*" program provided with the nmrPipe suite of programs, noise was added to this data set in the time domain and the corresponding spectra are shown on the left column, spectra (a), (d) and (g). Starting from the original HNCO, only 6 out of 18 projections ($\alpha_2^k = 7.5°, 22.5° \ldots$) were retained and processed; the corresponding spectra (c), (f) and (i) are shown on the right column. These 3 data sets were processed using our polar FT (upper row), the hybrid method (middle row) and the LV method (lower row). The peak amplitudes and shapes are not altered between spectra (a) and (b) as shown in the 1D cross-section. In contrast for LV and HBLV reconstruction, the increase of the noise strongly alters the weakest signals, for which intensities cannot be correctly quantified. Note the roundish shape of the peaks in (b) as compared to Cartesian acquisition in Figure 2b (the apodization function exhibits a circular symmetry) and the triangular shape (in e) and (h) of the partially overlapping signals even at high S/N ratio. For a small number of projection, aliasing due to undersampling leads to baseline oscillation in (c) which are centered around the observed cross-peaks. Similar patterns are present but at lower contour levels for HBLV and LV reconstruction.

in contrast to the polar FT (Figure 3a vs. 3b). This illustrates the different behavior of the two methods, the reconstruction being highly non linear and the polar FT strictly linear. As anticipated, the weak signals are more accurately reconstructed in spectra with higher S/N ratio. We have used the same apodization function for all spectra, i.e. for the 1D projections – before reconstruction – and along the radial direction – before polar FT. However, the cross-peaks in polar FT spectra are narrower (compare Figure 3b and 3e), although part of this follows from the requirement to sample 3100 Hz to enable the reconstruction of 2200 Hz.

When the number of projections is reduced, spectral artifacts that share the radial symmetry of the acquisition scheme become visible in the polar FT (see Figure 3c). These artifacts are oscillations with positive and negative amplitude, although only positive contours are plotted in Figure 3. It is noteworthy that the number of ridges per quadrant around a peak corresponds to the number of angular increments ($\alpha_2^k$). This pattern can be ascribed to the undersampling along the angular dimension for longer radial increments ($t_1^j$). At first glance, the LV and HBLV methods seem to be less sensitive to the small number of ($\alpha_2^k$) – at least using a first contour shown in Figure 3 – but the 2D baseline contains not only white noise but also similar geometric patterns if we go lower with regard to contour level.

Note that, even for a low number of projections, the line-width of the cross-peak remains narrower for the polar FT than for the reconstruction method. The artifacts shown for the polar FT are similar to those observed in the 1D spectra obtained with the Lagrange interpolation method (Marion, 2005) and clearly stem from geometric properties of the non-linear sampling scheme. Sarty (2003) has recently shown that sampling schemes that deliberately incorporate undersampled regions lead to aliasing artifacts (as illustrated by the point spread function) located far away from the parent peak. Their complete removal requires an *average* sampling density at the Nyquist density and is thus incompatible with a strict economy of data collection.

The presence of these ridges is clearly a drawback of this method. However, NMR spectroscopists are used to live with artifacts provided that they exhibit well-identified patterns. In this respect, *sinc* oscillations observed in FT spectra are illustrative: as their *complete* removal would require much stronger apodization function, it is common practice to leave them during processing: they can be later on filtered out by a peak picking routine which can account for their very characteristic geometrical signature (see for instance, the "*Sinc Detect*" option of nmrPipe (Delaglio et al., 1995)). In order to reduce the amplitude of the interferences while keeping the acquisition short, data-weighting techniques – as for undersampled MRI data (Pipe, 2000) – could be combined with the 2D polar FT. The polar FT is implemented as a *weighted* double sum (Equation 7) where the coefficients ($S^{jk} = S^j$) (Equation 10) should increase in a linear manner for radial increments. To minimize the artifacts in MRI due to a violation of the Nyquist sampling criterion (the sampling density is no longer high enough), Pipe invoked a weighting of the undersampled data according to the inverse of their density. This technique has been implemented by multiplying the time data by an apodization function $W^j$. We define an indice $j_0$ along the radial dimension; for $j < j_0$ the weighting coefficient $W^j = 1.0$ and for $j > j_0$, $W^j$ is reduced such that the product $W^j \times S^j$ remains constant ($= W^{j0} \times S^{j0}$). Figure 4 display the outcome of such weighting functions with $j_0 = 32$ and $j_0 = 16$ (for 128 radial increments). Minimizing the relative weight of the last data points reduces the artifacts but broadens the peaks. As in the case of data sampled in the Cartesian space, the choice of an optimal apodization function is a compromise between resolution and artifact containment. If this strategy is pushed further, the signal line-width converges asymptotically to that reported for a Cartesian sampling (Figure 2b). In conclusion, the improved resolution afforded by the radial sampling (for a given experimental time) is strictly correlated with the underlying violation of the Nyquist criterion. Conversely, the radial artifacts are the fine to pay for this violation.

Let us now compare our algorithm with that recently proposed by Kazimierczuk et al. (2006). Both methods aim at Fourier transform data with respect to more than one time variable and start from the same mathematical expression for two-dimensional integral (Equation 1 here and Equation 11 in Kazimierczuk et al. (2006)). However, their derived version for the discrete case leaves

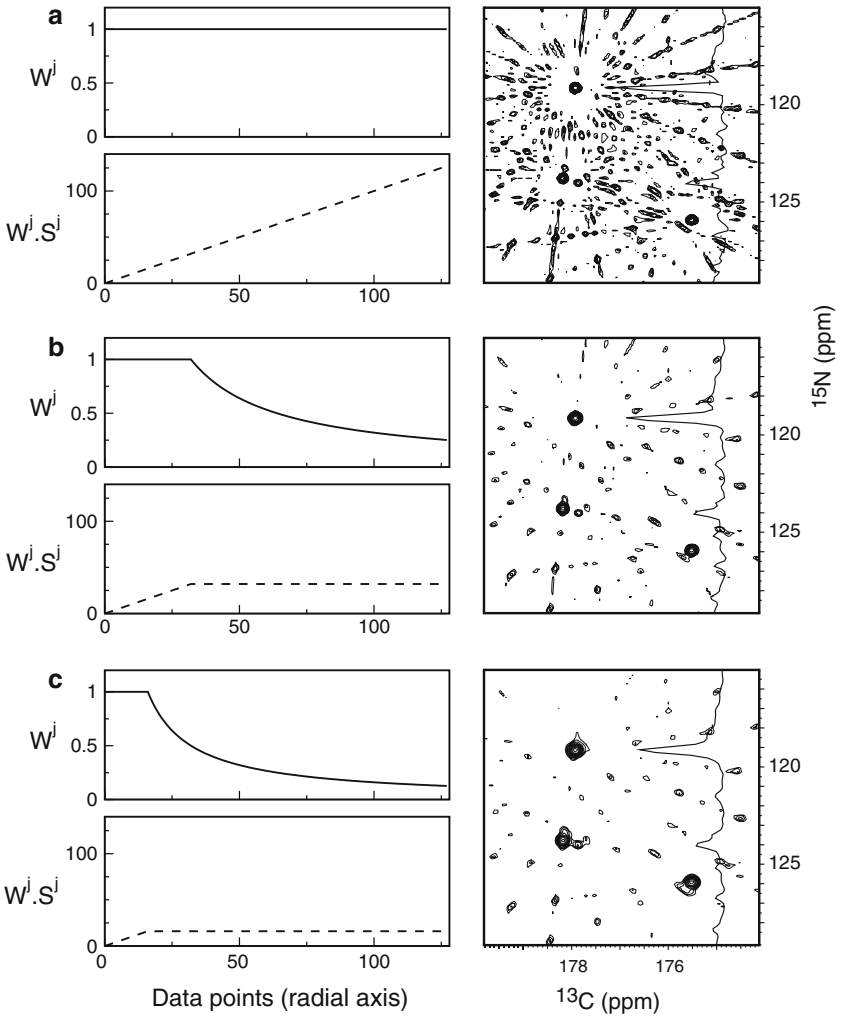


*Figure 4*. Influence of data weighting function for reducing artifacts. Apodization aims at lessening the contribution of the undersampled region (Pipe, 2000). The effect of 3 different functions $W^j$ is illustrated: in (a) $W^j = 1.0$ for all $j$, in (b) and (c) $W^j$ remains constant at the beginning of the signal (until $j_0 = 32$ and $j_0 = 16$, respectively) and decreases later on. In practice, the time-domain data are multiplied by $W^j \times S^j$, where $W^j$ is a "standard" apodization function and $S^j$ related to the integration area (Equation 10). For each processing, $W^j$ and $W^j \times S^j$ are shown on the left hand side (defined in arbitrary units) and the resulting spectrum on the right. As expected, this apodization smoothes out the data and thus reduces the aliasing artifacts (along with some white noise) at the expense of the peak line width.

out the integration area coefficients ($S^{jk}$ – cf. Equation 6) leading to the simplified expression:

$$\hat{F}(\nu_1^m, \nu_2^n) = \sum_{j=0}^{M-1} \sum_{k=0}^{N-1} f(t_1^j, \alpha_2^k) A_{jk}^{mn} \qquad (11)$$

Note that this approximation assumes a nearly linear acquisition scheme, where $S^{jk}$ is constant. In the case of radial acquisition, $S^{jk}$ increases linearly along the radial dimension (Equation 10 and Figure 1b); omitting this terms amounts here to scaling the data differently or, in other words, applying a apodization function defined as 1/t. The difference between the two implementations can be rationalized in the following manner. Focusing to the radial dimension, we are evaluating the following integral

$$F(\nu) = \int_{-\infty}^{\infty} t \cdot f(t) \exp(-2\pi i \nu t) dt \qquad (12)$$

while Kazimierczuk et al. are computing:

$$\hat{F}(\nu) = \int_{-\infty}^{\infty} f(t)\exp(-2\pi i\nu t)dt \tag{13}$$

A property of the Fourier transform (Arfken and Weber, 2005) states that, $F(\nu)$ is actually the derivative of $\hat{F}(\nu)$ (with a 90° phase shift). Let us move to the frequency domain and consider a typical liquid-state signal described by a Lorentzian shape centered at frequency $\nu_0$ and of line width $\Gamma$. Its absorptive and dispersive components ($A(\nu)$ and $D(\nu)$) are given by:

$$\begin{aligned} A(\nu) &= \frac{1}{\pi}\frac{0.5\cdot\Gamma}{(\nu-\nu_0)^2+(0.5\cdot\Gamma)^2} \\ D(\nu) &= \frac{1}{\pi}\frac{\nu-\nu_0}{(\nu-\nu_0)^2+(0.5\cdot\Gamma)^2} \end{aligned} \tag{14}$$

These expressions can be derived with respect to the frequency variable ($\nu$) leading to:

$$\begin{aligned} \frac{d}{d\nu}A(\nu) &= \frac{1}{\pi}\frac{(\nu-\nu_0)\Gamma}{\left[(\nu-\nu_0)^2+(0.5\cdot\Gamma)^2\right]^2} \\ \frac{d}{d\nu}D(\nu) &= \frac{1}{\pi}\frac{(0.5\cdot\Gamma)^2-(\nu-\nu_0)^2}{\left[(\nu-\nu_0)^2+(0.5\cdot\Gamma)^2\right]^2} \end{aligned} \tag{15}$$

Inspection of Equation 15 reveals that the derivative of one component exhibits the same symmetry as the other one: namely, the derivative of the dispersive component $d[D(\nu)]/d\nu$ is symmetrical with a narrow positive signal surrounded by two negative lobes (note that this is no longer a Lorentzian shape). Using these expressions, the line-width of the signal can be estimated as $\Gamma$ for the absorptive component and $0.484\times\Gamma$ for the derivative of dispersive component. Therefore, for Lorentzian shapes, the integral computed according to Equation 12 leads to narrower signals than using Equation 13, irrespective of the original spectral line-width.

Whereas the omission of the $S^{jk}$ coefficients (as proposed by Kazimierczuk et al., 2006) has no influence on signal positions, it strongly modifies the line-widths (assuming an identical apodization function) by a factor of two. Furthermore, as the first point is overestimated (as compared to the other ones), a positive dc offset is present (see Figure 3a of Kazimierczuk et al. 2006) which increases the signal integral. In contrast, with our method, the average of the artifacts due to the radial sampling is zero. In order to eliminate them (or at least make them less prominent), alternate acquisition schemes have to be designed. Kazimierczuk et al. (2006) have introduced a spiral sampling scheme (widely used in MRI) that leads to cleaner spectra: the choice of an angular increment which is not a integer fraction to $\pi/2$ eliminates the periodicity responsible of the pattern visible for radial sampling. In this case, it is difficult to anticipate the consequence of leaving out the $S^{jk}$ coefficients which express in a more complex manner.

Two last issues associated with the FT of polar data deserve further discussion: the quadrature detection and the Nyquist frequency. The sign detection along both dimensions requires the sampling of 2 signals ($x$, $y$) along each of them leading to a hypercomplex signal made of 4 components. In contrast to projection method, no linear combination to obtain zero- and double quantum coherence (Bersch et al., 2003) is necessary before processing. As far as the Nyquist sampling theorem, some local undersampling is necessary to reduce to experimental time and fully capitalize on radial acquisition. In contrast to Kazimierczuk et al. (2006) who emphasize the necessity to fulfill the Nyquist theorem using a global criterion ($sw_1\Delta t_1 + sw_2\Delta t_2 < 1$) along the two dimensions, a partial fulfillment along *both* dimensions at the beginning of the acquisition seems to be sufficient as shown in our previous paper (Marion, 2005).

## Conclusion

We have shown in this paper that the use of discrete Fourier transform is by no means limited to data sampled on a Cartesian grid according to the Nyquist sampling theorem. If rewritten in a different coordinate system with proper weighting of the experimental data, FT can virtually be applied to any sampling scheme. In this first account, we have compared this algorithm with reconstruction methods proposed in the literature. For the same data, much narrower signals can be obtained using polar FT, but aliasing artifacts become more visible for a small number of projections than in LV or HBLV methods. It should be said again that these artifacts are the

direct consequence of the violation of the Nyquist theorem and not of the implemented processing itself. The major advantage of the polar FT is its *linearity* which permits a quantitative interpretation of the spectra using the noise as a confidence estimate. It is likely that more sophisticated non-linear processing (such as MEM (Rovnyak et al., 2004) or FDM (Chen et al., 2004)) could yield better and/or cleaner spectra when used by experienced users, but the lack of any adjustable parameter in our method – except for apodization – makes it widely accessible to all NMR spectroscopists.

This general FT processing scheme opens up prospects for alternate data acquisition, because any timing can be handled. The sampling timing used here for the radial direction simply imitates the popular Fourier discretization scheme, i.e. on the zeros of a sine function ($z = N\pi$); Equation 7 could be rewritten as a Hankel/Bessel transform (Bracewell, 1999) for the radial component and thus the zeros of a Bessel function $J_0(\cdot)$ would probably be more logical (Myridis and Chamzas 1998). Kazimierczuk et al. (2006) have reported, with their evenly weighted method, an improvement when replacing polar sampling with spiral sampling, but this amounts more or less to spreading the artifacts over the entire spectral area. Our general FT algorithm is well suited as the framework for exploring new sampling schemes, as done recently in the field of MRI, to search for optimal compromise between experimental time, spectral resolution and moderate artifacts.

## Acknowledgment

The author would like to thank Dr. Frank Delaglio (NIH) for providing assistance and technical details on nmrPipe software.

## References

Arfken, G.B. and Weber, H.J. (2005) *Mathematical Methods for Physicists*,, Elsevier, Inc., Burlington, MA, USA, pp. 946–950.
Bersch, B., Rossy, E., Coves, J. and Brutscher, B. (2003) *J. Biomol. NMR*, **27**, 57–67.
Bodenhausen, G. and Ernst, R.R. (1982) *J. Am. Chem. Soc.*, **104**, 1304–1309.
Bracewell, R.N. (1999) *The Fourier Transform and Its Applications*, (3rd ed.). McGraw-Hill, New York, pp. 244–250.
Chen, J, Nietlispach, D., Shaka, A.J. and Mandelshtam, V.A. (2004) *J. Magn. Reson.*, **169**, 215–224.
Coggins, B.E., Venters, R.A. and Zhou, P. (2005) *J. Am. Chem. Soc.*, **127**, 11562–11563.
Delaglio, F., Grzesiek, S., Vuister, G.W., Zhu, G., Pfeifer, J. and Bax, A. (1995) *J. Biomol. NMR*, **6**, 277–293.
Gesmar, H., Led, J.J. and Abildgaard, F. (1990) *Prog. NMR Spectrosc.*, **22**, 255–288.
Kazimierczuk, K., Koźmiiski, W. and Zhukov, I. (2006) *J. Magn. Reson.*, **179**, 323–328.
Kupče, E. and Freeman, R. (2004a) *J. Am. Chem. Soc.*, **126**, 6429–6440.
Kupče, E. and Freeman, R. (2004b) *Concepts Magn. Reson.*, **22**, 4–11.
Kupče, E., Nishida, T. and Freeman, R. (2003) *Prog. NMR Spect.*, **42**, 95–122.
Malmodin, D. and Billeter, M. (2005) *J. Am. Chem. Soc.*, **127**, 13486–13487.
Marion, D. (2005) *J. Biomol. NMR*, **32**, 141–150.
Myridis, N.E. and Chamzas, C. (1998) *IEEE Trans. Med. Imag.*, **17**, 294–299.
Pipe, J.G. (2000) *Magn. Reson. Med.*, **43**, 867–875.
Rovnyak, D., Frueh, D.P., Sastry, M., Sun, Z.Y., Stern, A.S., Hoch, J.C. and Wagner, G. (2004) *J. Magn. Reson.*, **170**, 15–21.
Sarty, G.E. (2003) *Concepts Magn. Reson.*, **17B**, 17–24.
Simorre, J.P., Brutscher, B., Caffrey, M.S. and Marion, D. (1994) *J. Biomol. NMR*, **4**, 325–333.
Szyperski, T., Wider, G., Bushweller, J.H. and Wüthrich, K. (1993) *J. Am. Chem. Soc.*, **115**, 9307–9308.
Szyperski, T., Yeh, D.C., Sukumaran, D.K., Moseley, H.N. and Montelione, G.T. (2002) *Proc. Natl. Acad. Sci. USA*, **99**, 8009–8014.
Tugarinov, V., Muhandiram, R., Ayed, A. and Kay, L.E. (2002) *J. Am. Chem. Soc.*, **124**, 10025–10035.
Van Doren, S.W. and Zuiderweg, E.R.P. (1994) *J. Magn. Reson. B*, **104**, 193–198.
Van Melckebeke, H., Simorre, J.P. and Brutscher, B. (2004) *J. Am. Chem. Soc.*, **126**, 9584–91.
Venters, R.A., Coggins, B.E., Kojetin, D., Cavanagh, J. and Zhou, P. (2005) *J. Am. Chem. Soc.*, **127**, 8785–8795.
Yoon, J.W., Gosdsill, S., Kupče, E. and Freeman, R. (2006) *Magn. Reson. Chem.*, **44**, 197–209.